# Compression performance of composite plates after multi-site impacts: a combined experimental and finite element study

Spyridon Psarras[a,b,*], Raúl Muñoz[a,c], Mazdak Ghajari[a,d]

[a] *Dept. Aeronautics, Imperial College London, South Kensington campus, SW7 2AZ, UK*

[b] *Dept. of Mechanical Engineering and Aeronautics, University of Patras, 26500, Greece*

[c] *Departamento de Ingeniería Mecánica, Universidad de Salamanca, 37700, Spain*

[d] *Dyson School of Design Engineering, Imperial College London, South Kensington, SW7 2AZ, UK*

## Abstract

This paper reports on a study of the damage tolerance of carbon fibre reinforced polymer plates, used in aircraft fuselage, subjected to multi-site impacts. A new fixture was designed to perform sequential low-velocity impacts at different locations on plates with two different thicknesses, representing upper and lower fuselage panels. The residual strength in compression was measured using a new compression-after-impact rig designed to prevent global buckling of thin plates. Experimental results indicated that compared to single impacts, multi-site impacts can reduce the residual strength of the thin plates, but not the thick plates. To explain this difference, a detailed finite element model was developed, which enabled modelling of multi-site impacts and compression after impact in one simulation. Simulations suggested that the second impact damage changes the buckled shape prior to failure for the thin plates. A parametric analysis on key material parameters showed that they have a small effect on the residual compressive strength. This work can help to improve the design of aircraft panels with respect to

*Corresponding author
*Email address:* spsarras@upatras.gr (Spyridon Psarras)

threats posed by multi-site impacts.

*Key words:* A. Damage Tolerance, B. Impact Behaviour, C. Mechanical Properties, D. Nonlinear Finite Element Analysis, E. Polymer-matrix Composites

## 1. Introduction

Composite structures made of laminated carbon fibre reinforced polymers (CFRP) are used in modern aircraft. They can be subjected to low-velocity impacts during service, which may cause a significant loss of stiffness and strength in compression. The damage due to low energy, low velocity impact is one of the most dangerous types of impact damage since it is very difficult to detect during visual inspections if there is little evidence of damage on the external surface [1]. The main damages observed during low velocity impacts are matrix cracking parallel to the fibres, delamination due to interlaminar stresses and eventually, at higher energies, fibre breakage [2].

The vast majority of the studies on impact mechanics and residual strength of composites consider a single impact [3], [4], [5], [6], [7], [8], [9], [10], [11] or multiple impacts at the same location [12], [13], [14]. However, aircraft structures can be exposed to impacts at close but different locations, for example when they are under hail strike on the ground or during flight. Such impacts are referred to as multi-site impacts. There is very limited previous work on understanding the failure mechanisms of composite materials subjected to multi-site impacts and their influence on the residual strength of composite structures. One paper reported on single and multi-site impacts and compression-after-impact tests on composite plates made of AS4/3501-6 carbon fibre/epoxy material [15]. The impacts produced approximately 30 mm diameter damage in the specimens, measured by C-scan, and the distance between damage areas was 30 mm along the specimen mid-width axis (i.e., the damage sites were aligned with the loading direction). The stress concentrations due to an axial compressive load were observed with a thermal emission technique and showed little interaction between the damage sites. Moreover, the failure strain and failure load were nearly 14% higher for multi-site damaged specimens. Another investigation studied the effects of distance between two impact damage sites and their location with respect to the loading axis on the residual compressive strength of AS4/3501-6 carbon fibre/epoxy laminates [16]. When damage sites were aligned with the loading axis, the failure strain was slightly larger than the failure strain in single impacts. This agrees with the observations of [15]. However, for damage sites aligned transversely to the loading axis, the failure strain was significantly less than a single for small separation between the impact sites, but the failure strain approached the single impact case when the separation was increased. In another study, the effects of multi-site high velocity impacts, both sequential and simultaneous, were investigated on the delamination area and ballistic limit of glass/epoxy laminates [17]. An interesting observation was that in comparison with simultaneous impacts, sequential impacts caused larger damage and further reduction in ballistic limit. However both impacts showed significant reduction in the ballistic limit. These few studies show the significance of multi-site impacts, and the need for a good understanding of the parameters affecting the residual compressive strength after impact loading of CFRP materials.

The aim of this research is to determine the compressive behaviour of aircraft-grade carbon/epoxy laminates after suffering damage from multi-site impacts. Sequential multi-site impact tests were performed on composite plates with two different thicknesses, representing upper and lower fuselage of a commercial aircraft. During experiments, the impact load history was recorded and after each test, the extent of damage was determined with the C-scan method. After the impacts, the specimens were compressed up to failure and the failure loads were recorded. We tested whether the distance between impacts has a significant effect on reducing the compression after impact strength of the thin and thick plates. In order to better understand the failure mechanisms, detailed finite element (FE) models were used to predict impact damage and post-impact compressive strength and investigate the role of delamination in the compression after impact response of the plates.

Table 1: Lay-up and thickness of plates.

| material | name | lay-up | (thickness mm) |
|---|---|---|---|
| T800/M21 | thin | [±45, 90, 0, 90, 0, 90, ∓45] | 1.65 |
| | thick | [±45, 90, -45, 0, ±45, 0, 45, 0]s | 3.7 |

## 2. Methods

### *2.1. Composite plates*

Composite plates were manufactured using prepreg Hexcel T800-M21 plies of epoxy matrix reinforced with unidirectional carbon fibres. Two layups were used, one representative of a typical airliner upper fuselage (1.65 mm thick and designated as 'thin') and the other representative of a typical lower fuselage layup (3.7 mm thick and designated as 'thick'). The stacking sequence of each laminate is depicted in Table 1. The plates were manufactured by KVE Composites Group and their lamination quality was confirmed by using C-scans.

### *2.2. Impact test set-up*

Low velocity impact tests were performed using an Instron CEAST drop tower (Figure 1a). The size of each specimen was 100 mm wide by 150 mm in length. Each sample was placed in a rig located at the base of the tower. Four M20 bolts secured the upper and lower portion of the rig around the specimen and were tightened to 25 Nm. By using half-round support bars on both portions, the rig provided approximately simply supported boundary conditions for the plate on a 125 mm by 75 mm window (Figure 1b). The design of the rig allowed us to precisely control the location of the impact on the plate (Figure 1c). The plates were impacted with a hemispherical impactor of 20 mm diameter with a mass of 2.41 kg and an impact energy of 10 J, following the AITM 1-0010 [19]. The impactor was equipped with an accelerometer to record the force-time history.

As shown in Figure 1d, coupons were subjected to either one impact or a sequence of two impacts at different locations. According to NDT regulations, the minimum distance between impact centres must be 40 mm, so multi-site impacts were separated either 40 mm or 50 mm. The impacts were carried out at coordinates (-25,0) or (-25,0) & (15,0), or (-25,0) & (25,0) (mm from the center). Six specimens were tested for each impact scenario.

Damage in the specimens was inspected by using a Triton 1800 C-scan unit, manufactured by Tecnitest, equipped with piezoelectric probes of 10 Mhz and 5 Mhz. On selected specimens, a time-of-flight scan was also conducted in order to determine the location of the delaminations through the thickness.

In summary, the multi-site impact experiments were carried out in the following sequence:

1. Measurement and C-scan of the pristine coupons.
2. First impact during which the force time history was recorded.
3. C-scan inspection.
4. Second impact during which the force time history was recorded.
5. C-scan inspection.

For the single impact experiments, we performed steps 1 to 3 only.

### *2.3. Compression After Impact*

#### *2.3.1. A new fixture*

Following impacts on the plates, the Compression After Impact (CAI) strength was determined. A standard AITM 1-0010 fixture was used for thick plates, which has been shown to provide good results in previous work [19]. For thin plates, however, this fixture is not suitable because the specimen can fail due to local buckling at a location remote from the impact damage. To overcome this issue, a modification to the test fixture was designed which enabled the impacted specimen to be tested without buckling. This involved reducing the width between the vertical (longitudinal) knife edge supports and providing additional support to prevent buckling of the parts of the plate falling outside these knife edge supports. The adaptor includes two anti-buckling guides with minimal contact area with the specimen and a window to allow buckling of the plate at the location of delamination. The adaptor successfully focused buckling to the delamination sites and avoided premature buckling of the thin plates under compression (Figure 2a).

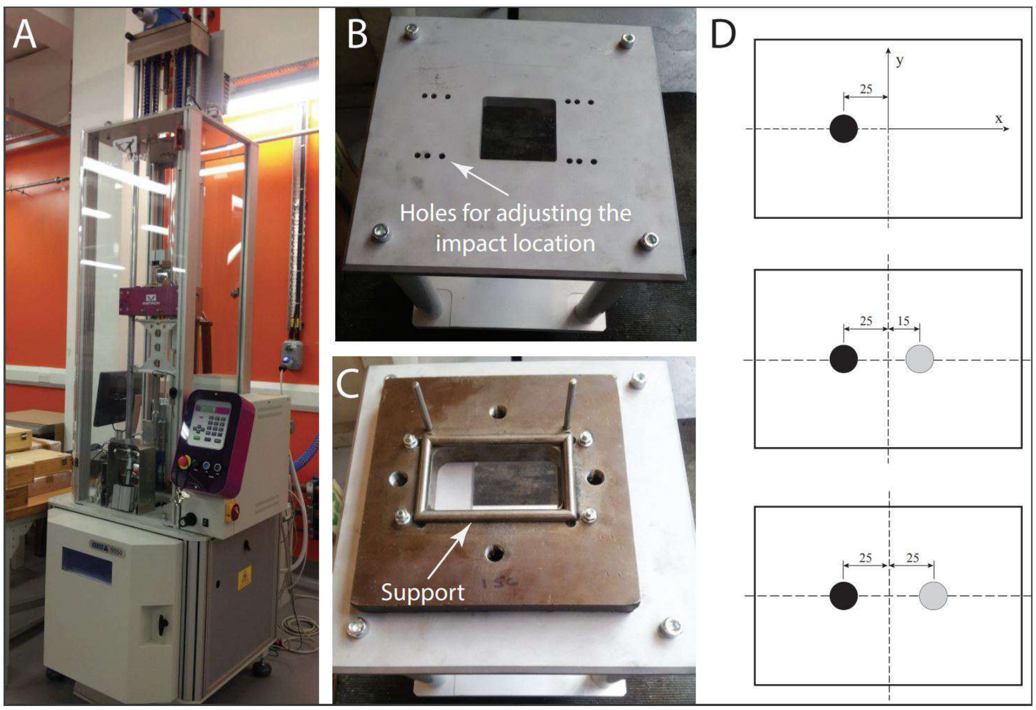


Figure 1: Impact set setup. a) Drop-weight tower. b) Lower support. c) Adapter plate designed to install the impact fixture with variable impact location. d) Location of single and multi-site impacts, shown with circles. Black indicates the first impact, whereas light grey indicates second impact. From top to bottom, (-25), (-25,+15) and (-25,+25) impact cases.

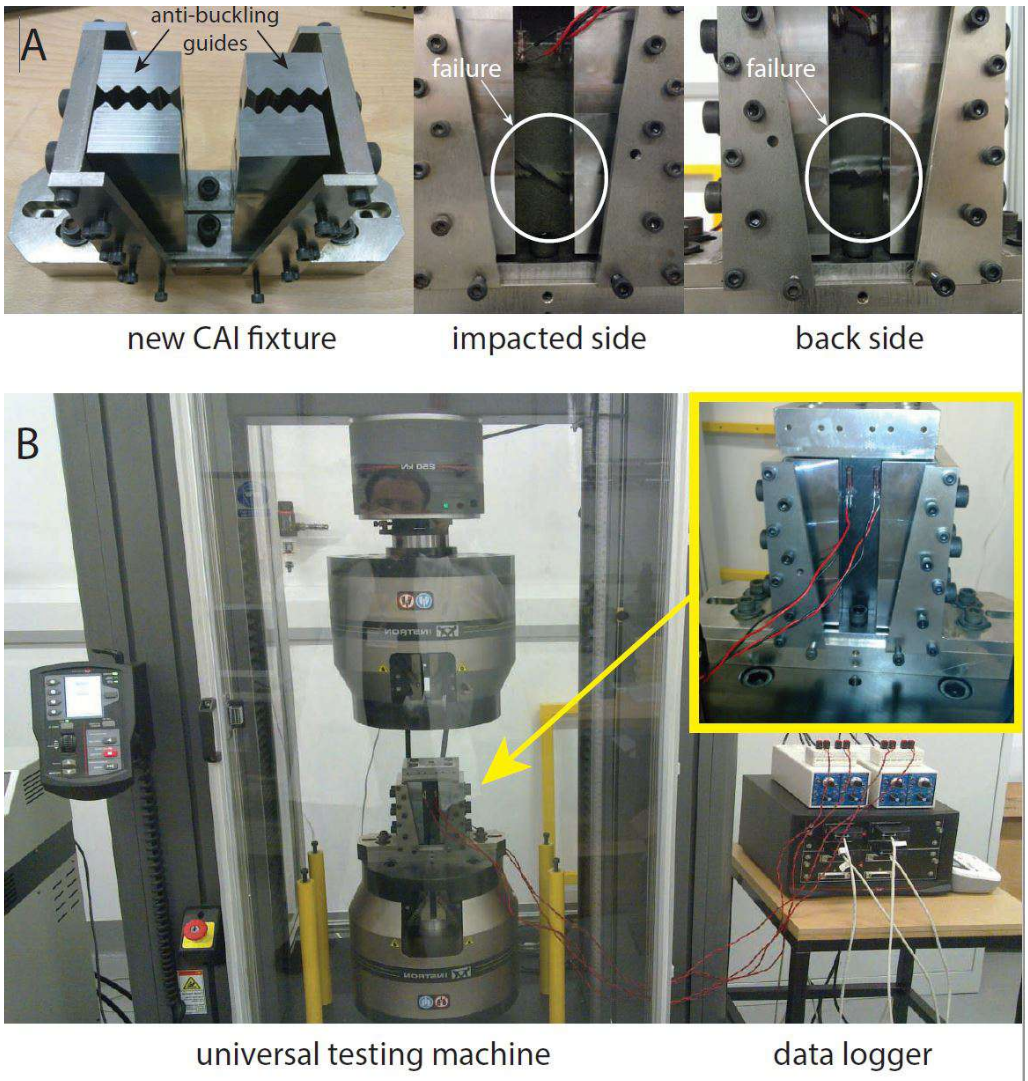


Figure 2: Compression after impact (CAI) experiments. (a) the new CAI fixture designed to avoid global buckling of thin plates. (b) CAI test setup.

#### 2.3.2. CAI test setup

Monotonic compression-after-impact tests were conducted in a universal testing machine (Instron) with a 250 kN load cell at a rate of 1.5 mm/min under displacement control by using a CAI fixture [? ]. A Linear Variable Differential Transducer (LVDT) was attached onto the lower loading plate to record the machine displacement (Figure 2b).

### 2.4. Finite Element Modelling

#### 2.4.1. Geometry and mesh

A Finite Element (FE) model based on a mesoscale approach was developed to simulate the CAI tests described in the previous section. The modelling of the impact and the subsequent CAI test was performed in a single combined FE analysis. FE models of the plates were created using one layer of continuum shell elements for each sub-laminate with two sub laminates chosen for the thin plate and four sub laminates for the thick case. Each sub-laminate of the plate was modelled with 8-node continuum shell elements with reduced integration (SC8R), whereas each ply within the sub-laminate was represented with a through-thickness integration point. This element type is particularly suitable for capturing plate bending and buckling. Damage within a ply was modelled using an energy-based user-defined subroutine.

Delamination damage (only at the interface between adjacent sub-laminates) was modelled using three dimensional cohesive elements. It was assumed that the properties of the cohesive layer are the same as the properties of the matrix. The number and location of cohesive layers are described in Table 2. Note that, in order to reduce the computational cost of simulations, cohesive layers were not introduced between every pair of plies, but only between sub-laminates.

The impact fixture was modelled including the contact between the specimen plate and the clamping fixture. The impactor was modelled as a rigid body. Vibration of the specimen after the impact were brought to zero using a viscous damping step. The baseline element size was 1 mm, which led to a total number of elements of approximately 55K for thin plates and 115K for thick plates.

Table 2: Number and location of cohesive layers on the baseline FE model

| plate | number of cohesive layers | lay-up of sublaminates |
|---|---|---|
| thin | 1 | sublam1: [±45, 90, 0, 90] |
| | | sublam2: [0, 90, ∓45] |
| thick | 3 | sublam1: [0, -45, 90, ∓45] |
| | | sublam2: [0, 45, 0, ∓45] |
| | | sublam3: [±45, 0, 45, 0] |
| | | sublam4: [±45, 90, -45, 0] |

#### *2.4.2. Constitutive models*

A constitutive model based on Continuum Damage Mechanics was implemented via a user-defined subroutine (VUMAT) in Abaqus Explicit to predict damage initiation and growth within each ply [20] [21]. This constitutive model incorporates four failure modes: tensile fibre fracture, compressive fibre fracture, coupled in-plane shear-tensile matrix fracture (quadratic criterion) and coupled in-plane shear-compressive matrix fracture. One feature of this model is that it has a non-linear curve for in-plane shear stress-strain. In addition, it can predict plastic strain during unloading. Furthermore, mesh objectivity is addressed within the implementation of this constitutive model. The material properties that were used in this constitutive model are presented in Table 3 and Table 4. For the cohesive elements, the well-established bilinear traction-separation model defined in Abaqus formulation was used.

#### *2.4.3. Multi-step analysis*

The multi-site impacts and compression after impact were modelled in a single analysis [22]. To achieve this, we developed a new procedure implemented in Python, which is described below.

Step 1 - impact: a sphere of 20 mm diameter, defined as a rigid body with a mass of 2.41 kg, is launched towards the plate with an initial velocity of 2.88 m/s. To replicate the experimental tests, the clamping fixture is explicitly modelled and hard contact is defined between the plate and the clamping fixture (Figure 3a).

Table 3: Ply properties used in the FE model (T800/M21). Subindices f, m, t and c stand for fibre, matrix, tension and compression, respectively. Material properties were obtained either from AIRBUS, experiments conducted at Imperial College London or from the literature [18].

| Parameter | Value |
|---|---|
| Ply thickness (mm) | 0.186 |
| Density (kg/m$^3$) | 1580 |
| Elastic properties (GPa) | $E_{11} = 139$, $E_{22} = 8.1$ |
| | $G_{12} = 5.1$, $\nu_{12} = 0.33$ |
| Strength (MPa) | $X^T = 2900$, $X^C = 1660$, $Y^T = 58$ |
| | $Y^C = 25$, $S = 95$ |
| Fibre fracture toughness (kJ/m$^2$) | $G_{ft} = 184$, $G_{fc} = 100$ |
| Matrix fracture toughness (kJ/m$^2$) | $G_{mt} = 0.303$, $G_{mc} = 0.303$, $S^L = 0.1$ |

Table 4: Cohesive parameters used in the FE model.

| Parameter | Value |
|---|---|
| Thickness $T_0$ (mm) | 0.186 |
| Density (kg/m$^3$) | 1300 |
| Penalty stiffness (kN/mm$^3$) | $K_n = 200$ |
| | $K_s = K_t = 100$ |
| Normal interface strength (MPa) | 50 |
| Shear interface strength (MPa) | 95 |
| $G_{Ic}$ (J/m$^2$) | 765 |
| $G_{IIc}$ (J/m$^2$) | 1250 |
| Benzeggah-Kenane parameter | 2.0 |

Step 2 - damping: Viscous damping is applied between each impact on the whole structure as if it were immersed in a viscous liquid. The damping force generated is proportional to the velocity of every node. The value of the damping coefficient $C_v$ selected was 1% of the quantity $\rho C_d$, where $\rho$ is the material density and $C_d$ the wave speed of the material. This procedure enabled us to dissipate the kinetic energy of the plate after the impact. Steps 1 and 2 were repeated for each impact.

Step 3 - compression: once the vibration in the plate is damped out, it is compressed in the longitudinal direction at a rate of 1.5 mm/min.

#### *2.4.4. Anti-buckling guides*

The Compression After Impact behaviour of thin laminates is particularly susceptible to geometric imperfections. As plates are usually not perfectly flat, contact between the anti-buckling guides and the plate is discontinuous, which makes straight bars unsuitable for predicting the response of the laminate. Hence, anti-buckling guides with a wavy shape were included in the FE model. They were modelled with shell elements as perfectly rigid. A wavelength of 9 mm was used and a penalty contact was defined between the outer surface of the plate and the anti-buckling guide. For thick plates, lateral displacement of thick coupons was constrained in a set of nodes parallel to the longitudinal edge.

## 3. Results

### *3.1. The multi-site impact response of thin and thick plates*

For thin plates, the impact test results were very consistent across all 6 tests, regardless of the impact location. The peak impact force was $4.5 \pm 0.2$ kN and the duration of impacts was $5.8 \pm 0.2$ ms. The impact force had a small drop near the peak, indicating the onset of delamination (Figure 4a). The thin plates showed elongated, elliptical damage at each impact site (approximately 20 mm major axis aligned with splitting of the 45° plies visible on the back surface of the panel). The second impact did not change the size of the delamination caused by the first impact.

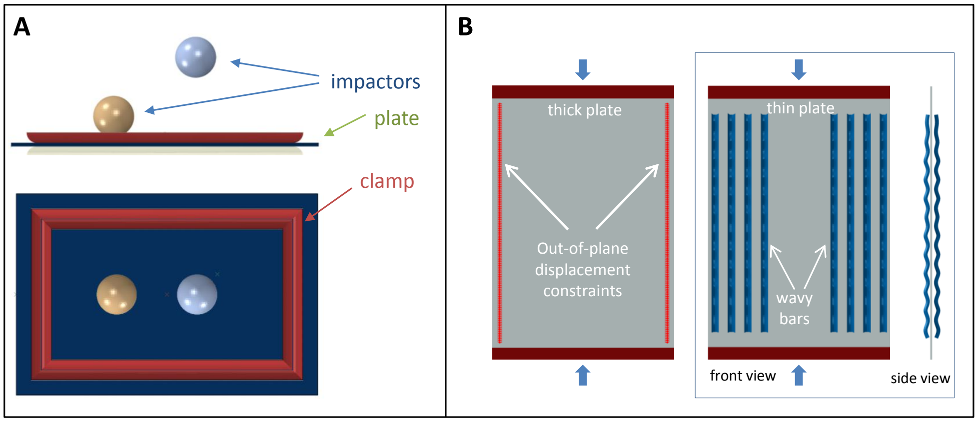


Figure 3: (a) FE model of the multi-site impact test. Impacts take place sequentially at two different locations. Contact is defined between the clamping fixture and the plates. (b) Boundary conditions during CAI tests. The out-of-plane displacement of thick plates is constrained along the contact line with the knife edge supports, whereas wavy anti-buckling guides were modelled for thin plates.

The impact test results were also consistent for the thick plates. The peak force was 6.0 $\pm$ 0.3 kN and the duration of impacts was 2.9 $\pm$ 0.1 ms. The impact force temporarily dropped at around 0.7 ms, indicating the onset of damage (Figure 4b). Similar to the thin plates, C-scan inspection revealed that the damage caused by the impacts was localised at the impact site with no overlapping or interaction between the damages. The shape of the damage produced by the impacts was approximately circular, with no visible damage on the back surface and a diameter of 20 $\pm$ 0.2 mm. In both cases the 20 mm damage size that was set by Airbus as the minimum damage requirement was met.

### *3.2. The residual compressive strength of the plate*

For thick plates, CAI tests showed that the load-displacement curve was linear until shortly before failure, regardless of the number of impacts (Figure 5). For thin plates, the load-displacement curve was slightly nonlinear, especially the (-25,+25) case. The final collapse of all laminates occurred in an abrupt manner and was triggered at the impact locations. The associated damage always passed through one of the impact locations.

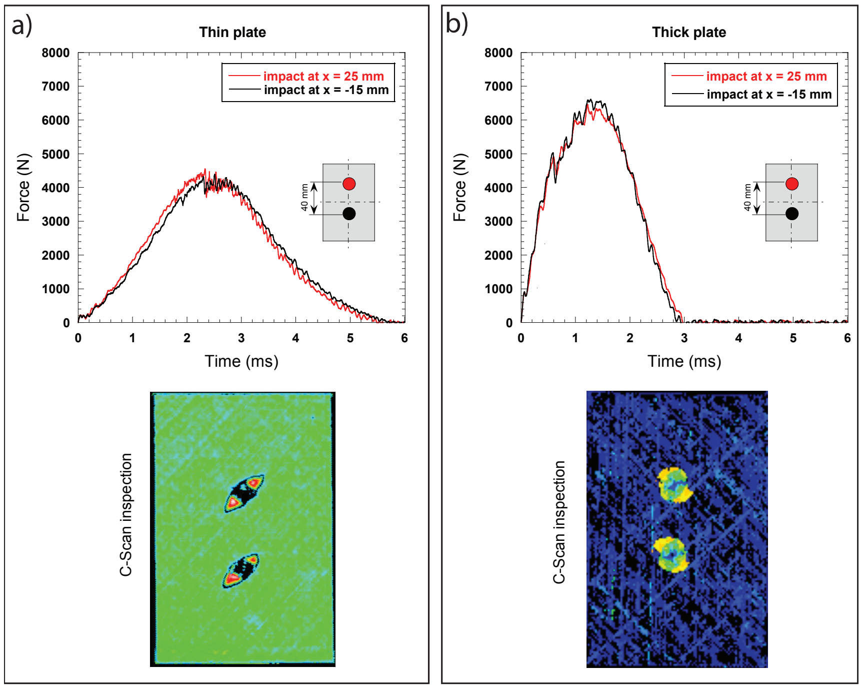


Figure 4: Experimental force-time curves and C-scans of representative specimens subjected to a sequence of two impacts at (-25,+15). a) thin plates and b) thick plates.

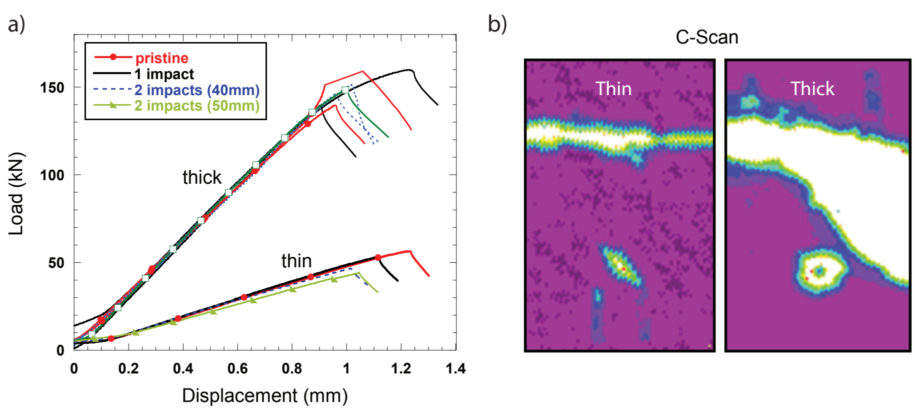


Figure 5: (a) Representative CAI curves of 4 loading scenarios. (b) C-scan images of specimens impacted at (-25,+15).

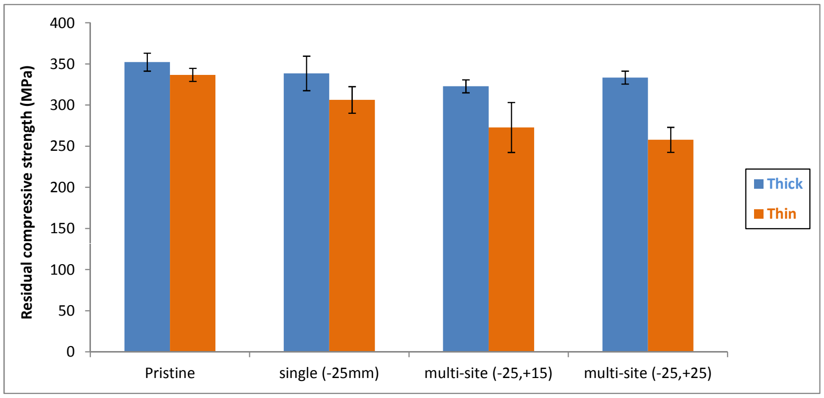


Figure 6: Average residual compressive strength and standard deviation of pristine, single impact and double impact plates. Thin plates are in orange and thick plates are in blue.

The residual compressive strength of the thin pristine plates was 336.8 ± 5.6 MPa . After a single impact, the compressive strength was reduced to 306.3 ± 16.1 MPa (a 9% reduction in mean). After multi-site impacts at (-25,+15), the residual compressive strength was further reduced to 272.8 ± 30.3 kN (19% reduction in mean compared to pristine plates). Compared to the single impacts, according to a statistical t-test analysis, this reduction was not significant (t=1.689, p=0.167). After multi-site impacts at (-25,+25), the residual compressive strength was reduced to 257.8 ± 15.2 MPa (23% mean reduction compared to pristine plates). Compared to the single impacts, this reduction was significant (t=3.788, p=0.019 - 16% reduction in mean). Although increasing the distance between the multi-site impacts slightly reduced the residual compressive strength of the thin plates, this reduction was not significant (t=2.776, p=0.486). The CAI tests on the thin panels showed the two-site impacts caused larger reductions (11% and 16% for the 40mm and 50mm separation cases respectively) in the average strength compared to a single impact. The scatter in the results (especially in the 40 mm separation case) indicates that the reduction is not statistically significant for the 40 mm separation case but is significant for the 50 mm separation case.

The residual compressive strength of the thick pristine plates was 352.2 ± 7.5 MPa. After a single impact, the compressive strength was reduced to 338.5 ± 21.0 MPa (a 4% reduction in mean). After multi-site impacts at (-25,+15), the residual compressive strength was further reduced to 322.9 ±

7.9 MPa (8% reduction in mean compared to the pristine plates). Compared to the single impacts, this reduction was not significant (t=2.776, p=0.292). After multi-site impacts at (-25,+25), the residual compressive strength was 333.4 ± 7.9 MPa (5% reduction compared to the pristine plates). The residual compressive strength was not significantly different to that in single impacts (t=2.776, p=0.712). Increasing the distance between the multi-site impacts did not have a significant effect on the residual compressive strength (t=2.776, p=0.176). The CAI tests on the thick panel revealed two-site impacts caused a small reduction (8% and 5% for the 40 mm and 50 mm separation cases, respectively) in the average strength compared to a single site impact, However, the scatter in the results indicates that this reduction was not statistically significant for both cases of two-site impact.

A summary of the residual compressive strength of both thin and thick plates is depicted in Figure 6.

### *3.3. Finite element predictions*

#### *3.3.1. Predicting the impact response of the thin and thick plates*

The FE model predicts a temporary drop in the force at around 2.6 kN and 3.1 kN for the thin and thick plates, respectively (Figure 7). These force drops were associated with delamination initiation and growth in the cohesive layers at the site of impact. Simulations showed damage in the matrix of the sub-laminates, but not fibre damage. This matrix damage was greater on the rear side of the coupon than on the front due to the higher tensile stresses caused by bending. The FE predictions of force and damage size and pattern were not significantly influenced by the number of impacts or impact location, in agreement with the experiments.

The maximum contact force predicted was in good agreement with experimental data for thick plates (less than 2% error). The predicted location and pattern of damage were in agreement with C-scan observations for both thick and thin plates. However, the delamination size was overestimated by the FE model, especially for thin plates

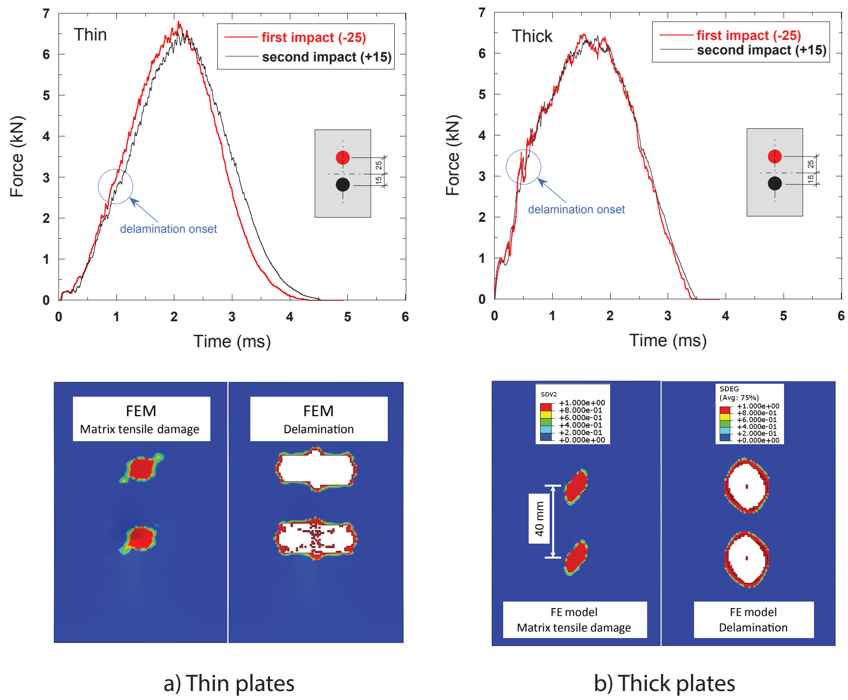


Figure 7: Force-time curves and matrix damage predicted by the FE model after (-25,+15) impacts for (a) thin plates and (b) thick plates. No fibre damage was observed.

#### *3.3.2. Predicting the compression after impact response of the thin and thick plate*

The FE models predicted a linear load-displacement up to failure for thick plates and slightly non-linear behaviour for thin plates, in agreement with the experimental data (Figure 8).

As can be seen in Figure 9, failure initiates from one of the sites damaged by the impact and propagates perpendicularly to the loading direction. At the failure load, three damage mechanisms, namely fibre breakage, delamination and matrix tensile cracking, are triggered. Interestingly, both simulation and experimental data show that there was no interaction between the two impact-damage areas during compression.

The predicted compressive strength of the plates is compared to the experimental data in Table 5. For the CAI of the thin plates the predicted failure load for the single impact case was in very good agreement with average experimental value. However, the predicted failure loads for the two site impact cases were almost identical to the single impact case (and approximately 18% higher than the experimental average values). The prediction of the compression strength of the pristine case was also 14% higher than the experimental value. Again, the predicted damage growth initiated from only one of the impact sites in the two-site impact cases as was observed in the experiment). For the CAI of the thick plates the predicted failure loads were close to the experimental average values (5%-8% higher) and reflected the insignificant loss in strength of the two-site impact case compared to the single site case. However, the prediction of the compression strength of the pristine case was 30% higher than the experimental value. In the cases of two-site impact the damage growth initiated from only one of the impact sites as was observed in the experiment.

The relative difference between the predicted compressive strength and mean value of the experimental results varied between 5% to 21%. The best predictions were made for plates damaged by a single impact. However, the FE model overestimates the residual strength of the pristine coupons, where the relative error rises up to 21% for thick plates. Despite this difference, the FE model predicts a strength reduction in both plates as a result of impacts, in agreement with experiments.

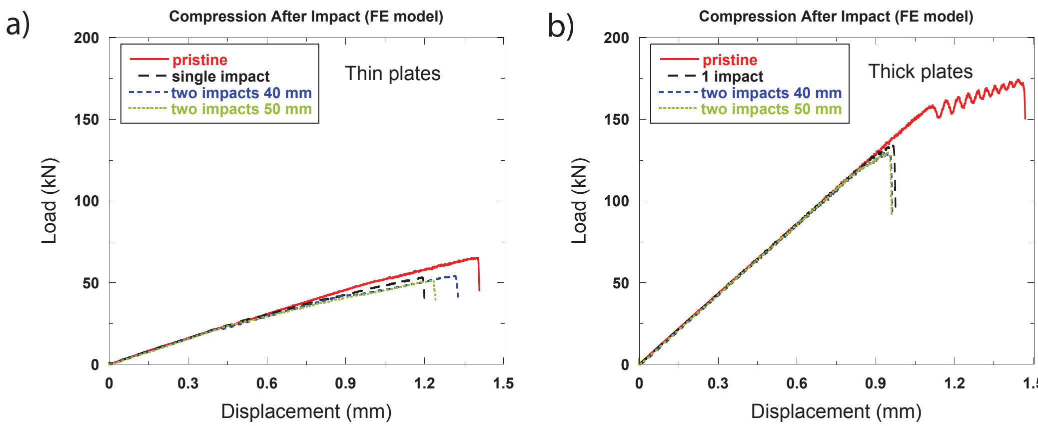


Figure 8: Load-displacement curves predicted by the FE model for (a) thin and (b) thick plates.

Table 5: Compressive strength ($X_c$) of thin and thick coupons. Experimental *vs* numerical results.

| | thin | | | thick | | |
|---|---|---|---|---|---|---|
| | $X_c$ (MPa) | | $\varepsilon_r$ (%) | $X_c$ (MPa) | | $\varepsilon_r$ (%) |
| | exp | fem | | exp | fem | |
| pristine | 336.8 ± 5.6 | 393.9 | 14 | 352.2 ± 7.5 | 459.5 | 21 |
| one impact (-25) | 306.3 ± 16.1 | 321.2 | 5 | 338.5 ± 21.0 | 362.2 | 7 |
| two impacts (-25,+15) | 272.8 ± 30.3 | 327.3 | 17 | 322.9 ± 7.9 | 351.4 | 8 |
| two impacts (-25,+25) | 257.8 ± 15.2 | 315.2 | 18 | 333.4 ± 7.9 | 351.7 | 5 |

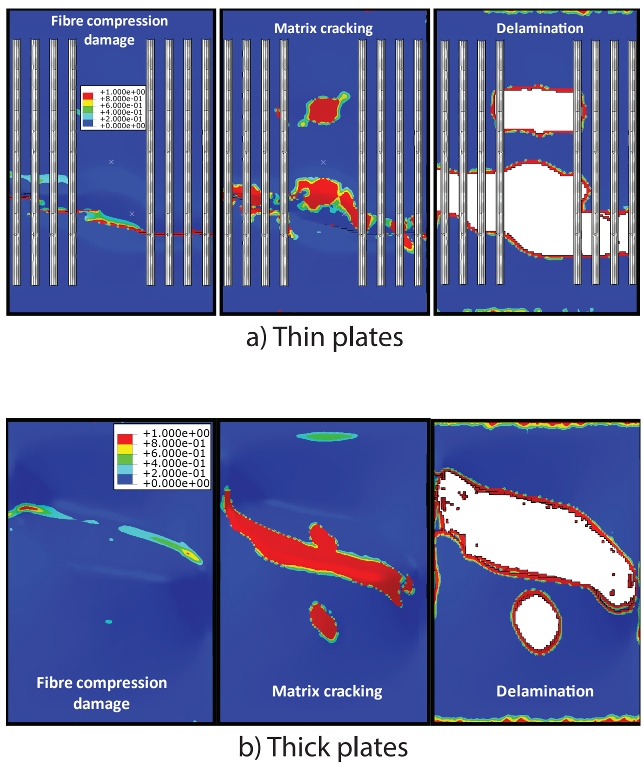


Figure 9: Damage predicted by the FE model after compression of (a) thin and (b) thick plates. Results correspond to the (-25,+15) impact case.

Table 6: Material properties used in the parametric analysis. The variable modified in each test is represented in bold.

| load case | Xc (MPa) | $G_{fc}$ (kJ/$m^2$) | $G_{IIc}$ (kJ/$m^2$) |
|---|---|---|---|
| baseline | 1660 | 100 | 1.25 |
| lower Xc | **1328** | 100 | 1.25 |
| lower $G_{fc}$ | 1660 | **80** | 1.25 |
| lower $G_{IIc}$ | 1660 | 100 | **1.0** |

### *3.3.3. The effects of material properties on impact and compression response*

Physically-based failure models, such as the one applied in this study, require a set of input parameters which are difficult to accurately determine. Having observed the differences between the FE predictions and the experimental results, a small study was performed to investigate the sensitivity of the FE predictions to key material properties. This may explain some of the differences that are observed between the FE predictions and experiments. In order to determine the effects of key parameters of the constitutive models on predicted compressive strength of the plates, a sensitivity analysis was performed. In turn, the values of the ply compressive strength ($X_c$), ply fracture toughness in compression ($G_{fc}$) and mode II interlaminar fracture toughness ($G_{IIc}$) were lowered by 20% (Table 6) and predicted the response of the plate to impacts and compression to failure.

The analysis revealed that the FE model is not very sensitive to such modifications. For thin plates, the maximum compressive strength reduction is 8% and it occurs for the (-25,+15) impact case due to a reduction of the ply compressive strength $X_c$. For thick plates, Figure 11 indicates that the mode II interlaminar fracture toughness ($G_{IIc}$) has the largest effects, with a slight increase in the delaminated area and a 8% strength reduction for the (-25,+25) impact case. The influence of $X_c$ and $G_{fc}$ on the residual compressive strength of thick plates is negligible.

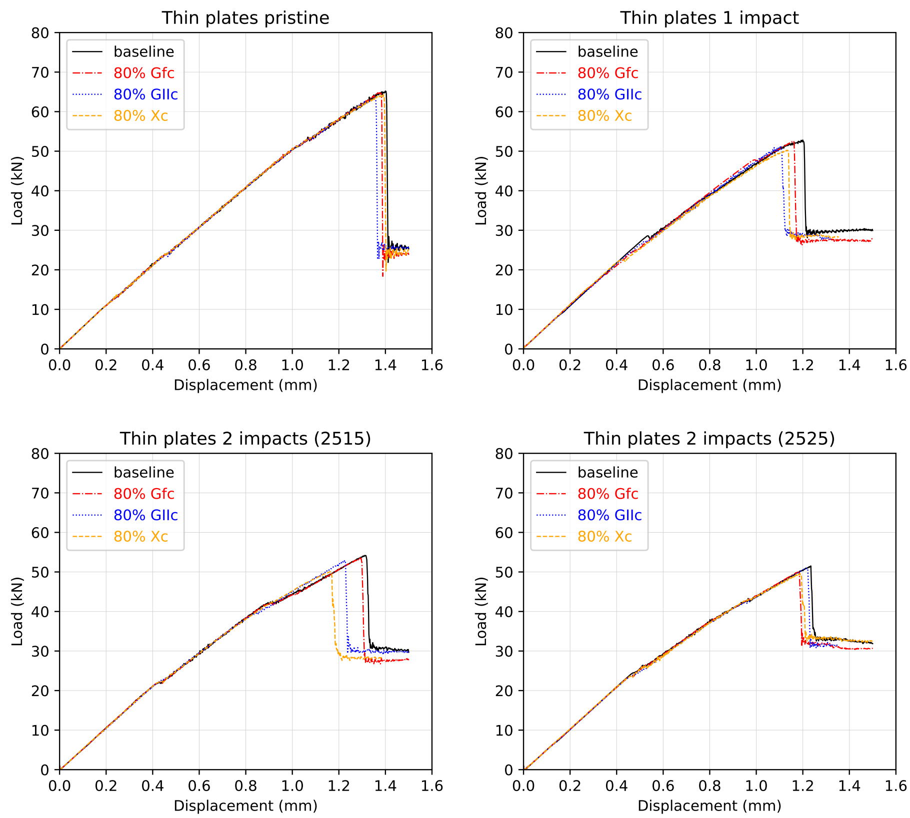


Figure 10: Load-displacement curves of thin plates predicted by the FE model for each loading scenario. Comparison of baseline model with a 20% reduction of 3 material properties: fibre fracture toughness in compression $G_{fc}$, interlaminar fracture toughness in mode II $G_{IIc}$ and compressive strength $X_c$.

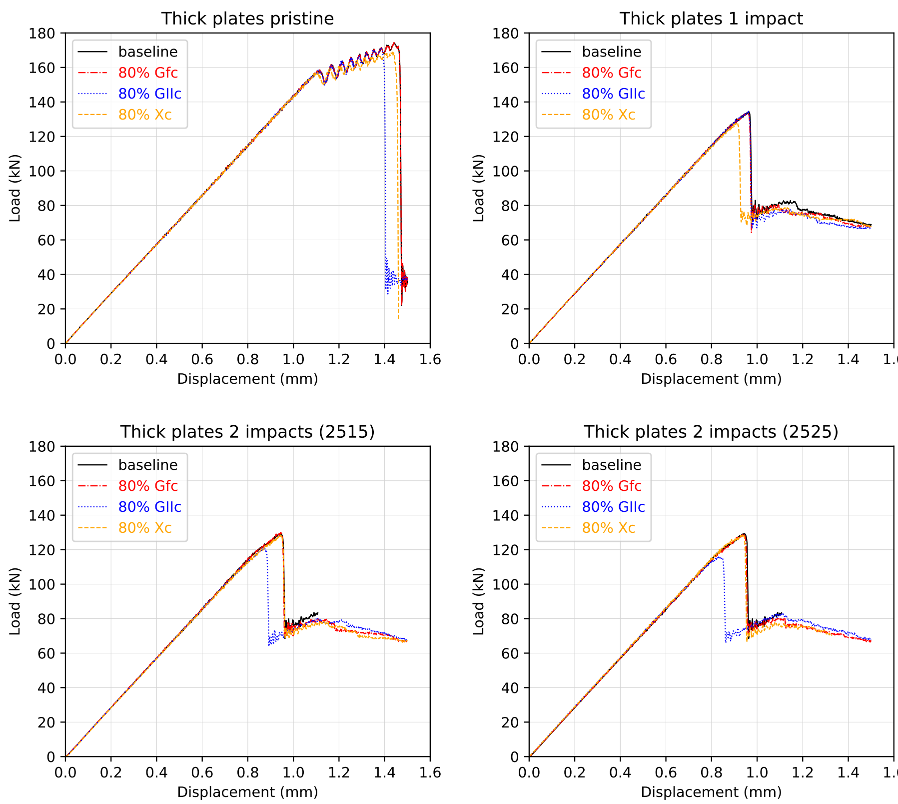


Figure 11: Load-displacement curves of thick plates predicted by the FE model for each loading scenario. Comparison of baseline model with a 20% reduction of 3 material properties: fibre fracture toughness in compression $G_{fc}$, interlaminar fracture toughness in mode II $G_{IIc}$ and compressive strength $X_c$.

## 4. Discussion

Our experimental results show that compared to single impacts, multi-site impacts may reduce the residual compressive strength of CFRP composite plates used in aircraft fuselage design. For the thin plates tested here (intended to be representative of upper fuselage panels of an airliner), the CAI strength was reduced by 16% due to second impact when this was 50 mm from the first impact. However, the second impact did not have a significant effect on reducing the compressive strength of the thick plates (representative of lower fuselage panels).

Three key factors are likely to have large effects on the performance of thin and thick plates subjected to double-site impacts: damage interaction, delamination size and buckling shape. In this study the impact sites were far apart so that no interaction between impact damages were observed during compression. It is likely that reducing the distance between impacts will lead to interaction between the damage areas. The impacts were along the loading axis (tandem configuration). The increase of the delaminated area caused by the second impact could reduce compressive strength, but the tandem configuration of the impacts meant that the effective cross section of the plate was almost unaffected by the second impact. In addition, for thick plates the second impact did not cause a significant strength reduction, despite of the increase in the delaminated area.

Buckling and post-buckling deformation of the plates were examined by means of the FE model. As shown in Figures 12 and 13, ultimate failure of the laminates occurs at the impacted regions and is not caused by global buckling. Results indicate that the peaks of the out-of-plane displacement prior to failure, which are represented as elliptical regions in blue and red colours, vary depending on the number of impacts and plate thickness. For thin plates, as the number of impacts increases from 1 to 2, the number of peaks increases from 2 to 4. This suggests that the second impact may trigger a transition to a higher buckling mode (Figure 12). For thick plates, impacted coupons exhibit only one out-of-plane displacement peak (Figure 13), regardless of the number of impacts, so there is no change in the buckling shape prior to failure.

Thus, it can be concluded that when the impact energy of the second impact is sufficiently high to cause a permanent out-of-plane displacement (indentation) and thus modify the buckled shape, the residual compressive strength can be significantly reduced.

Our detailed FE model, which modelled multi-site impacts and compression after impact in one simulation, was able to predict the residual strength of the plates with an acceptable accuracy. It predicts a strength reduction of 3% for thick plates as a result of the second impact, regardless of the location. This is in agreement with experiments, where the second impact causes a further reduction in strength between 2% and 5% depending on the impact location. However, the FE model overestimated the residual strength of the pristine coupons, where the relative error rises up to 21% and 14% for thick and thin plates, respectively (Table 5). This can be due to the following reasons:

- The mechanical behaviour in compression of composites during experimental tests is quite sensitive to flaws, fibre misalignment and lack of flatness. As the FE model has none of these imperfections, it overpredicts the compressive strength of the laminate.
- The low number of cohesive layers, which makes the laminate stiffer. This can be solved by adding more cohesive layers, but at the expense of a higher computational cost.
- It was assumed that contact between the CAI fixture and thick coupons was perfect, but contact occurs only at certain locations. Recalling that the FE model of thin plates includes anti-buckling guides with some waviness rather than straight, this might explain the better results found for the pristine thin coupons.

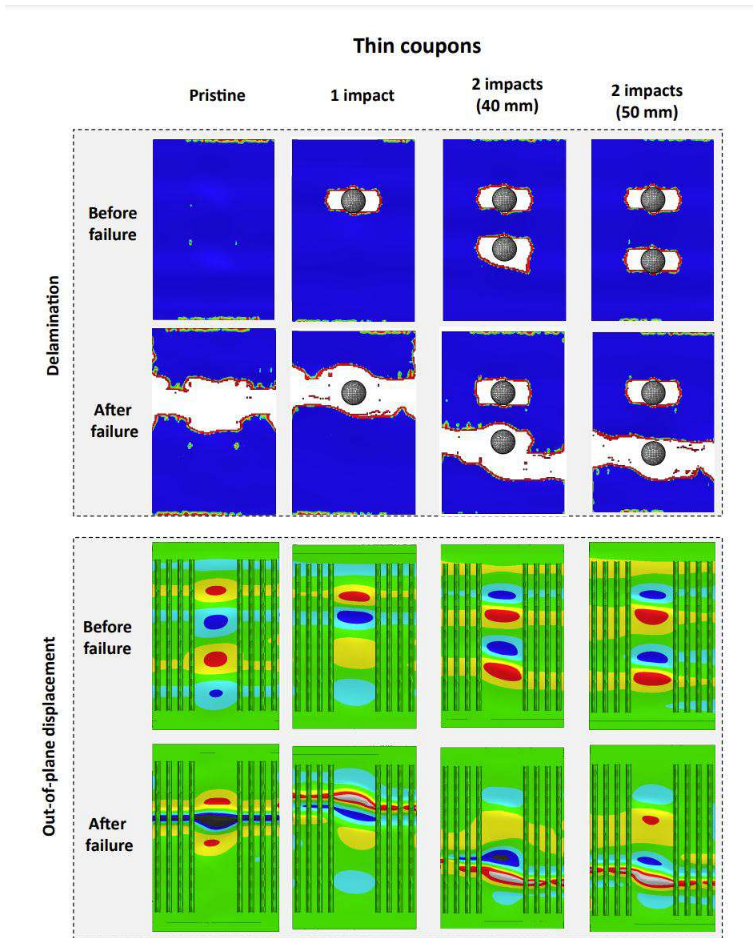


Figure 12: Delamination and out-of-plane deformation observed in simulations right before and right after failure of thin coupons.

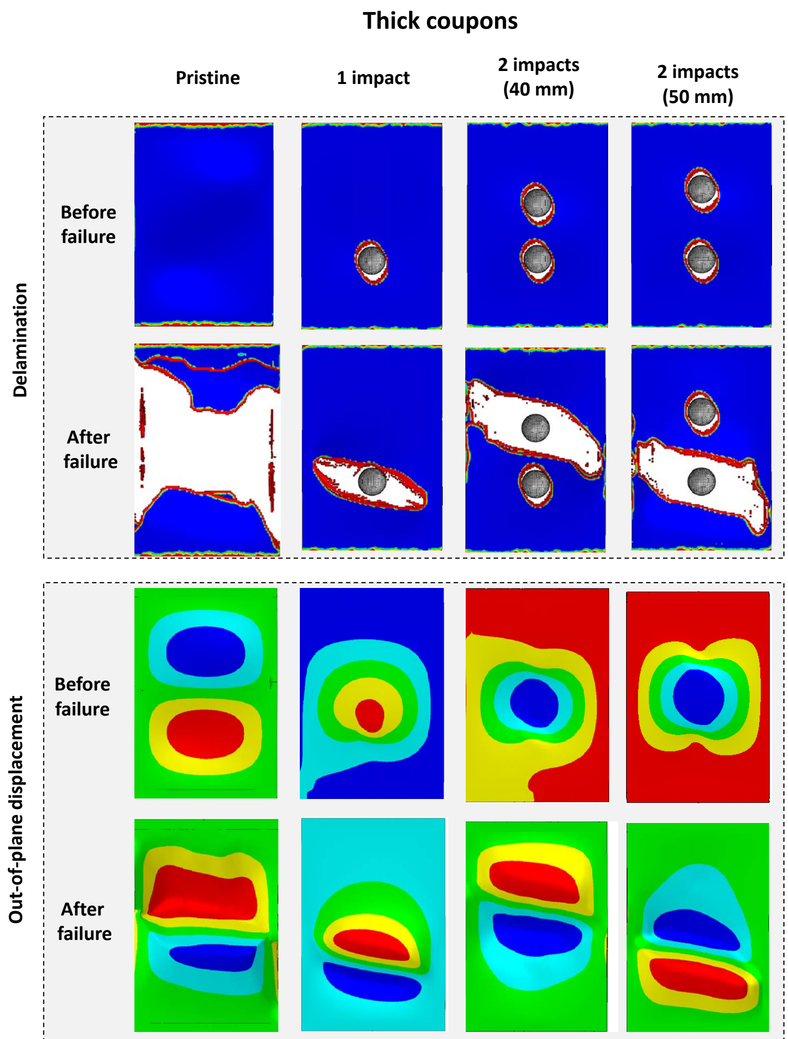


Figure 13: Delamination and out-of-plane deformation observed in simulations right before and right after failure of thick coupons.

## 5. Conclusions

In summary, we determined the residual compressive strength of thin and thick composite plates under single and multi-site impacts using new CAI fixtures and detailed FE models. The main conclusions of this study are:

- A novel fixture has been validated for conducting multi-site Compression After Impact tests and avoiding global buckling of thin plates.
- The contact force histories of the first and second impacts were almost identical and no interaction was found between damaged sites, which suggests that impacts can be studied independently.
- For thin plates, the second impact leads to a significant residual compressive strength reduction, which is likely due to modification of the buckling shape prior to failure. For thick plates, impact energies were not sufficient to reduce the residual compressive strength.
- A new FE modelling approach has been presented, which predicts the residual compressive strength of impacted coupons with an acceptable relative error lower than 18% and 8% for thin and thick coupons, respectively. Such methodology is a valuable tool for simulating more complex structural components, such as stiffened composite fuselage panels, as the sublaminate approach reduces the model size and computational time, about 4 times in this study.
- According to the parametric analysis, modest reductions of the interlaminar fracture toughness in Mode II, ply compressive strength and fibre fracture toughness in compression, do not affect significantly the residual compressive strength.

## 6. Acknowledgements

This project has received funding from the European Union's Seventh Framework Programme for research, technological development and demonstration under grant agreement no 284562.

We thank Domenico Furfari, from Airbus Operations GmbH in Hamburg, for support.

## References

[1] M de Freitas and L Reis. Failure mechanisms on composite specimens subjected to compression after impact. *Composite Structures*, 42(4):365–373, aug 1998. https://doi.org/10.1016/S0263-8223(98)00081-6

[2] M O W Richardson and M J Wisheart. Review of low-velocity impact properties of composite materials. *Composites Part A: Applied Science and Manufacturing*, 27(12):1123–1131, jan 1996. https://doi.org/10.1016/1359-835X(96)00074-7

[3] X.C. Sun and S.R. Hallett. Failure mechanisms and damage evolution of laminated composites under compression after impact (CAI): Experimental and numerical study. *Composites Part A: Applied Science and Manufacturing*, 104:41–59, 2018. https://doi.org/10.1016/j.compositesa.2017.10.026.

[4] Tuo, H.; Lu, Z.; Ma, X.; Xing, J. and Zhang, C. Damage and failure mechanism of thin composite laminates under low-velocity impact and compression-after-impact loading conditions. *Composites Part B: Engineering*, 163:642–654, 2019. https://doi.org/10.1016/j.compositesb.2019.01.006

[5] S. Hernandez, F. Sket, C. Gonzalez, J. LLorca, Optimization of curing cycle in carbon fiber-reinforced laminates: Void distribution and mechanical properties. *Composites Science and Technology*, 85:73–82, aug 2013. https://doi.org/10.1016/j.compscitech.2013.06.005

[6] M. Sadighi, M. Yarmohammad Tooski, R.C. Alderliesten. An experimental study on the low velocity impact resistance of fibre metal laminates under successive impacts with reduced energies. *Aerospace Science and Technology*, 67:54–61, sep 2017. https://doi.org/10.1016/j.ast.2017.03.042

[7] Leif E Asp, Sören Nilsson, and Sunil Singh. An experimental investigation of the influence of delamination growth on the residual strength of impacted laminates. *Composites Part A: Applied Science and Manufacturing*, 32(9):1229–1235, sep 2001. https://doi.org/10.1016/S1359-835X(01)00075-6

[8] D D R Cartié and P E Irving. Effect of resin and fibre properties on impact and compression after impact performance of CFRP. *Composites Part A: Applied Science and Manufacturing*, 33(4):483–493, apr 2002. https://doi.org/10.1016/S1359-835X(01)00141-5

[9] Emile Greenhalgh, Charlotte Meeks, Andrew Clarke, and James Thatcher. The effect of defects on the performance of post-buckled CFRP stringer-stiffened panels. *Composites Part A: Applied Science and Manufacturing*, 34(7):623–633, jul 2003. https://doi.org/10.1016/S1359-835X(03)00098-8

[10] G.A.O. Davies, D. Hitchings, T. Besant, A. Clarke, and C. Morgan. Compression after impact strength of composite sandwich panels. *Composite Structures*, 63(1):1–9, 2004. https://doi.org/10.1016/S0263-8223(03)00119-3

[11] Andrey Shipsha and Dan Zenkert. Compression-after-Impact Strength of Sandwich Panels with Core Crushing Damage. *Applied Composite Materials*, 12(3):149–164, may 2005. http://dx.doi.org/10.1007/s10443-005-1119-1

[12] J. Jefferson Andrew, V. Arumugam, K. Saravanakumar, H.N. Dhakal, C. Santulli. Compression after impact strength of repaired GFRP composite laminates under repeated impact loading. *Composite Structures*, 133:911–920, 2015. https://doi.org/10.1016/j.compstruct.2015.08.022

[13] Ercan Sevkat, Benjamin Liaw, Feridun Delale, and Basavaraju B Raju. Effect of repeated impacts on the response of plain-woven hybrid composites. *Composites Part B: Engineering*, 41(5):403–413, jul 2010. http://dx.doi.org/10.1016/j.compositesb.2010.01.001

[14] A. M. Amaro and P. N.B. Reis and M. F.S.F. De Moura and M. A. Neto. Influence of multi-impacts on GFRP composites laminates. *Composites Part B: Engineering*, 52(9):93–66, 2013. https://doi.org/10.1016/j.compositesb.2013.03.041

[15] R Jones. Residual strength of composites with multiple impact damage. *Composite Structures*, 28(4):347–356, jan 1994. https://doi.org/10.1016/0263-8223(94)90117-1

[16] S C Galea and W K Chiu. The effect of multiple impact damage on the residual compressive strength of composite structures. *International Journal of Crashworthiness*, 1(3):305–314, jan 1996. https://doi.org/10.1533/cras.1996.0023

[17] L J Deka, S D Bartus, and U K Vaidya. Multi-site impact response of {S2}-glass/epoxy composite laminates. *Composites Science and Technology*, 69(6):725–735, may 2009. https://doi.org/10.1016/j.compscitech.2008.03.002

[18] M Laffan, S Pinho, P Robinson & A McMillan. Translaminar fracture toughness testing of composites: A review. *Polymer Testing*, 31:481–489, jan 2012. https://doi.org/10.1016/j.polymertesting.2012.01.002

[19] AITM 1-0010. Airbus Test Method. Determination of Compression Strength After Impact. 2005.

[20] S. Psarras, T. Loutas, G. Galanopoulos, G. Karamadoukis, G. Sotiriadis, and V. Kostopoulos. Evaluating experimentally and numerically different scarf-repair methodologies of composite structures. International Journal of Adhesion and Adhesives, pp. 102495, 2019.

[21] L Iannucci and M L Willows. An energy based damage mechanics approach to modelling impact onto woven composite materials—Part I: Numerical models. *Composites Part A: Applied Science and Manufacturing*, 37(11):2041–2056, nov 2006. https://doi.org/10.1016/j.compositesa.2005.12.013

[22] 7. S. Psarras, T. Loutas, G. Galanopoulos, G. Karamadoukis, G. Sotiriadis, and V. Kostopoulos. Compression After Multiple Impacts: Modelling and Experimental Validation on Composite Coupon Specimens. Smart Intelligent Aircraft Structures, Chapter 31, 2016, Springer, (ISBN:978-3-319-22412-1).